FATIGUE BEHAVIOR OF WELDED BEAMS

Manfred A. Hirt, Howard, Needles, Tammen and Bergendoff; and
John W. Fisher, Lehigh University

The fatigue behavior of welded steel beams is evaluated by using the fracture-mechanics concepts of stable crack growth. A fracture-mechanics model for cracks originating from the pores in the web-to-flange fillet weld is developed. Estimates of the stress-intensity factor are made that numerically describe the initial flaw condition. With the final crack size known, a theoretical crack-growth equation was derived from the fatigue test data of the welded beams. The derived relationship compares well with actual crack-growth measurements on a welded beam and available data from crack-growth specimens. The regime of crack growth, where most of the time is spent growing a fatigue crack in a structural element, is shown to correspond to growth rates below 10^{-6} in. per cycle. Few experimental crack-growth data are available at this level. It is concluded that the fracture-mechanics concepts can be used to analyze fatigue behavior and to rationally evaluate the major variables that influence the fatigue life of welded beams.

•THIS paper evaluates the fatigue behavior of welded steel beams without attachments by using the fracture-mechanics concepts of stable crack growth. Earlier studies had indicated that various flaw conditions existed in welded beams. Both internal and external weld defects in the web-to-flange fillet weld were evaluated and discussed in detail elsewhere (4, 9, 10). Internal pores caused by entrapped gas in the weldment are known to form a common defect. The gas pores and their effect on the fatigue behavior of welded beams are discussed in this paper.

A fracture-mechanics model for cracks originating from the pores in the web-to-flange fillet weld is developed. Estimates of the stress-intensity factor are made that numerically describe the initial flaw condition. With the initial and final crack size known, a theoretical crack-growth equation was derived from the fatigue test data of the welded beams. The experimental data of 56 plain-welded beams covering three grades of steel—ASTM A 36, A 441, and A 514—are presented elsewhere (4, 9) together with an analysis of the test variables.

Fracture toughness was not a significant factor in the determination of crack propagation and the fatigue life of the beams tested. Net-section yielding generally terminated fatigue testing. Hence, no emphasis was placed on this aspect of failure because it was not relevant to the study. Fracture toughness can become a problem when steel with low toughness is used and adverse environmental and load conditions exist. These limitations were not the subject of this investigation.

The main objective of this paper is to demonstrate the validity and applicability of fracture-mechanics concepts of fatigue crack growth to the fatigue behavior of actual structural elements containing real flaws. It is also shown that the ΔK-values responsible for crack growth in these beams are well below the ΔK-values normally obtained during crack-growth testing. A theoretical crack-growth equation was derived from the fatigue life data of welded beams and compared with available crack-growth data.

Sponsored by Committee on Steel Superstructures.

The following notation is used in this paper:

C = a material related constant in crack-growth equation;
K = elastic stress-intensity factor for a crack (ksi$\sqrt{\text{in.}}$);
N = number of applied stress cycles;
N_{ij} = number of cycles required for a crack to grow from size a_i to size a_j;
S = nominal applied stress in the extreme fiber of the tension flange;
S_r = stress range;
a = crack size, crack radius for penny-shaped crack, half-crack width for tunnel crack or through-the-thickness crack, crack depth for surface crack, crack radius for corner crack, minor half axis for elliptical crack;
a_e = equivalent radius of a penny-shaped crack that provides the same K-factor estimated for the arbitrarily shaped crack;
a_f = final crack size;
a_i = initial crack size (for integration interval);
a_j = final crack size (for integration interval);
b = major half axis for an elliptical crack;
f(a) = nondimensional geometry correction factor for stress-intensity factor K;
n = exponent of crack-growth equation; slope of equation in log-log transformation;
α = (n/2) - (1);
ΔK = stress-intensity factor range;
$\Delta\sigma$ = stress range relevant for the determination of the stress-intensity factor range; and
σ = stress applied sufficiently away from the crack tip.

FATIGUE STRENGTH OF WELDED BEAMS WITH INTERNAL WELD DISCONTINUITIES

It was observed that cracks in the welded beams always originated from a discontinuity (flaw) in the web-flange fillet weld unless a severe notch existed at the flame-cut flange tip. More than 180 cracks were found in the plain-welded beams reported on elsewhere (4, 9). Seventy-five of these cracks were cut open for fractographic examination. It was found that about 80 percent of the cracks had originated from porosity caused by the entrapment of gas. In general, these cavities were completely inside the weld. The gas pores appeared on the fracture surface as rounded cavities with a smooth and shiny surface as shown in Figure 1. A few pipe or blow holes extended to the surface of the weld.

All test data for beams failing from porosity in the longitudinal fillet weld are plotted by the solid circles shown in Figure 2. The equation of the mean line resulting from a least squares fit to these test data is

$$\log N = 10.3528 - 2.9844 \log S_r \qquad (1)$$

Previous analyses (4, 9) had indicated that stress range was the dominant variable and that grade of steel did not significantly affect the fatigue strength.

The open symbols shown in Figure 2 represent plain-welded beams that failed from defects other than porosity. This included beams failing from weld repairs, stop-start positions, other weld defects, and severe notches in the flame-cut flange tips. Generally, these beams yielded shorter lives than did beams failing from porosity.

When weld repairs were absent in the fillet weld of beams with stiffeners or attachments, failure occurred at these welded details because they were more critical than was porosity. These beam data are also included because they revealed no visible crack growth in the longitudinal fillet weld at lower stress ranges. An indication of a run out level is seen at the 18-ksi stress-range level. Only three data points from plain-welded beams failing from porosity were observed at that stress range.

CRACK-GROWTH OBSERVATION ON A PLAIN-WELDED BEAM

One plain-welded beam was closely observed in order to investigate crack formation and growth on the surfaces of the fillet weld, web, and flange. Measurements of crack

length and load were made so that crack-growth rates could be determined for the structural element and compared with the crack-growth relationship analytically derived from the S-N data of the welded beams. Beam PWB-341 (4) was selected for this study because it had failed prematurely after 192,000 cycles of stress from a flange-tip crack. Replicate beams tested at the same stress range of 36 ksi indicated that a crack from a gas pore could be expected to become visible within an additional 200,000 cycles. The flange-tip crack was carefully repaired, and testing was resumed under the same stress conditions. The fillet welds on both sides of the web in the constant moment region were searched for cracks by using a regular hand magnifying glass while testing at 250 cycles per minute. Testing was interrupted periodically so that the weld could be examined under static load. Suspicious locations were further examined with a 50-power microscope.

A hairline crack was first detected on the weld surface after a total of 351,700 applied stress cycles. The apparent total crack size visible on the weld surface was found to measure about 0.05 in. when the load was removed from the beam. This increased to 0.25 in. under maximum stress of 50 ksi in the extreme fiber. Only the linear dimension of the crack on the fillet weld could be observed during continued testing until the crack reached the extreme fiber.

After about 435,000 cycles, the crack was first detected on the bottom surface of the flange. It was only then observed with certainty that the crack had also penetrated through the other fillet weld. The increase in crack size was very rapid after the crack had penetrated the bottom flange surface. The cross section of the flange fractured at 467,000 cycles as one crack tip reached the flange tip. The advancement of the crack is shown in Figure 3, which indicates a transition from a penny-shaped crack with a continuous crack front in the flange-web junction to a three-ended crack with two crack tips in the flange and one in the web.

Hence, two basic stages of growth were observed for cracks originating from pores in the longitudinal fillet weld of welded beams. The first stage of growth was in the flange-to-web junction from the initial crack size (flaw) up to the point where the crack reached the extreme fiber of the flange. After penetration of the extreme flange fiber, the crack changed its shape rapidly to become a three-ended crack.

A PENNY-SHAPED CRACK MODEL

Fractographic examination of small cracks that had originated from pores in the fillet weld showed that many were almost perfectly circular in shape. This circular shape was found at various stages of growth up to the point where the crack had reached the extreme fiber of the flange, as shown in Figures 4, 5, and 6.

One of the smallest cracks was discovered during an examination of a crack in the fillet weld. A tiny crack about 0.07 in. in diameter had originated from a very small pore in the left weld as shown in Figure 4. The extent of the circular crack is seen from the smooth crack surface surrounding the pore, as compared to the rough appearance caused by static tearing when the cross section was opened for inspection. The small crack on the left was completely inside the flange-to-web junction and could not be detected by inspection of the weld surface.

A small crack discovered by the magnetic particle inspection method is shown in Figure 5. The crack had initiated from the elongated pore and grown to the surface of the fillet weld. Almost no deviation from a circular shape is visible. This crack is about 0.26 in. in diameter and could not be detected on the weld surface with the aid of a magnifying glass even under favorable circumstances and under sustained loading.

A crack that has nearly penetrated the extreme fiber of the tension flange is shown in Figure 6. Again, no significant disturbance of the circular shape is apparent at either side of the web or at the front approaching the surface of the flange. This crack, although quite sizable, is not easily detected on a structural element under applied loading. The linear dimension of the crack visible on the surface of the flange-to-web junction is somewhat less than 1 in.

The phenomenon of a circular crack shape, seemingly not influenced by the free surfaces, is believed to be a result of the compatibility condition of the basically

Figure 1. Examples of porosity from the root of the longitudinal fillet weld.

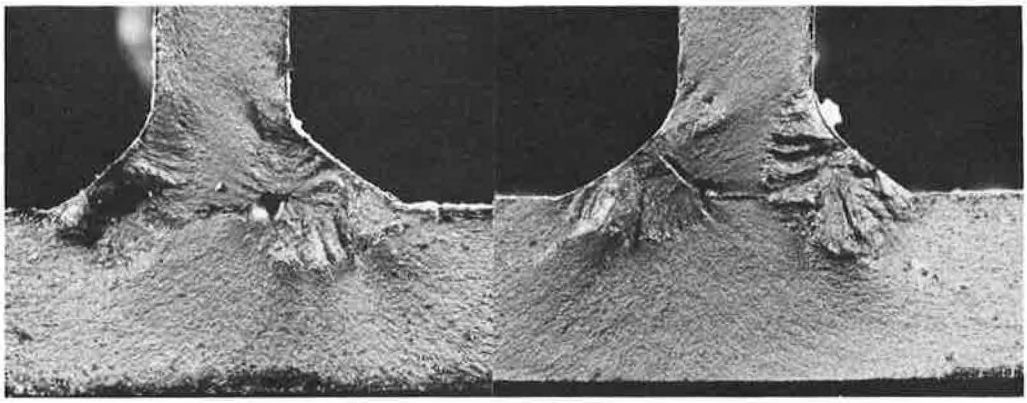

(a) Typical gas pore (x2.5)

(b) Pore elongated and perpendicular to the weld surface (x2.5)

Figure 2. Comparison of welded beams failing from porosity in the fillet weld with beams failing from other defects.

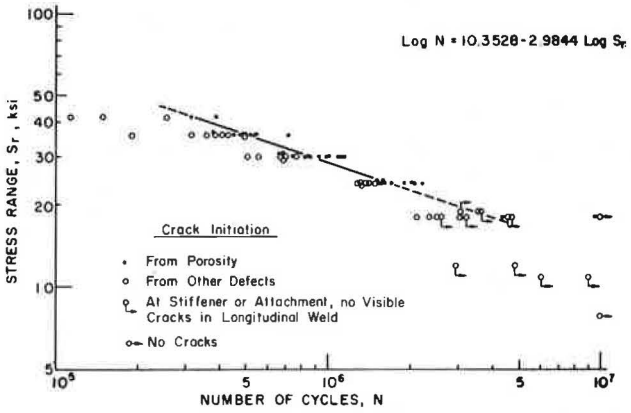

Figure 3. Stages of crack growth from a pore in the fillet weld.

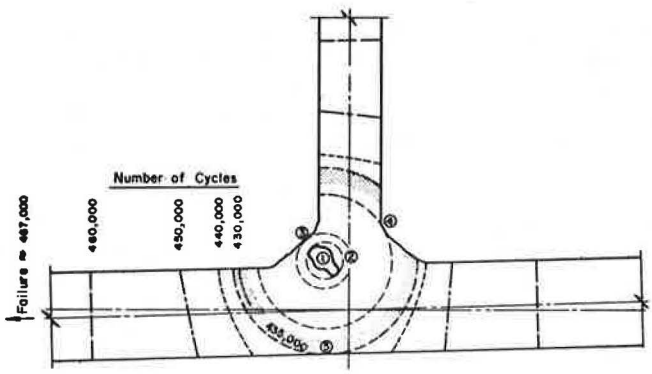

elastic cross section. Based on this photographic evidence, a circular disc-like crack was assumed to model the actual crack during growth inside the flange-web connection (Fig. 3).

EVALUATION OF FATIGUE BEHAVIOR USING FRACTURE-MECHANICS CONCEPTS

The fatigue test data and fractographic observations of small fatigue cracks suggested that fracture mechanics of stable crack growth might be useful in evaluating the observed behavior of the test beams. The stress intensity factor K introduced by Irwin (11) describes in convenient form the influence of the stress, applied sufficiently away from the crack tip, and the crack size, a. The relative size is usually expressed in terms of a correction function, f(a), where the linear dimensions of the plate, or the distance to a free edge or surface, are introduced.

$$K = \sigma\sqrt{\pi a}\, f(a) \quad (\text{ksi}\sqrt{\text{in.}}) \tag{2}$$

Paris (15) has suggested the following relation between the rate of crack propagation and the change in the stress-intensity factor:

$$da/dN = C\Delta K^n \tag{3}$$

This model expresses crack growth per cycle, da/dN, in terms of the variation of the stress intensity factor, ΔK, and two material constants, C and n.

For the case of a crack with constant correction factor, f(a), which is subjected to constant amplitude stress, integration of Eq. 3 yields

$$N_{ij} = (1/C)\left[(1/\alpha f(a)^n\, \pi^{n/2}\, \Delta\sigma^n)\,(a_i^{-\alpha} - a_j^{-\alpha})\right] \tag{4}$$

where $\alpha = (n/2) - (1)$. For specimens with equal initial crack size, a_i, final crack size, a_j, and identical boundary conditions, a theoretical value for the prediction of the life interval, N_{ij}, can be expressed in terms of a new constant, C', times the applied stress range, $\Delta\sigma$, as

$$N_{ij} = C'\,\Delta\sigma^{-n} \tag{5}$$

where

$$C' = (1/C)\left[(1/\alpha f(a)\,\pi^{n/2})\,(a_i^{-\alpha} - a_j^{-\alpha})\right] \tag{6}$$

The log-log transformation of Eq. 5 yields a straight line in the form

$$\log N_{ij} = \log C' - n \log(\Delta\sigma) \tag{7}$$

APPLICATION TO THE PLAIN-WELDED BEAM

For the application of the outlined concepts of fracture mechanics, a reasonable characterization of the flaws was needed. A large number of cracks that originated from porosity in the fillet weld were examined closely to establish the initial flaw condition. Flaws were photographed and enlarged to at least four times, as shown in Figure 1. The dimensions of the defects were measured on the photographs under 10-power magnification.

Pores were examined in beams fabricated from three different grades of steel (A 36, A 441, and A 514). K-values were estimated to numerically describe the measured flaw dimensions. The estimated K-values describing the pores were obtained by using a circumscribed ellipse for flaws similar to the shapes shown in Figure 1a and Figure 6. For elongated flaws comparable to those shown in Figure 1b and Figure 5, the K-estimate at the narrow transition from the circular void to the elongated pore was generally used.

It was previously concluded from fractographic inspection of very small fatigue cracks (Figs. 4 and 5) that a penny-shaped crack model described the shape of cracks during crack growth. However, the estimated K-values for the initial flaws represent

elliptical shapes with various a-b ratios. Hence, each individual defect was transformed into a penny-shaped crack with an "equivalent crack-radius, a_e," corresponding to the estimated K-value. An average equivalent crack radius, $a_e = 0.04$ in., was selected from the sample to represent the collection of measured pores. The initial crack radius, a_i, was then assumed equal to this average value.

Derivation of Crack-Growth Constants

The coefficients of the crack-growth equation can now be established from the equivalence of the coefficients in Eqs. 1 and 7. Equation 7 is the theoretical prediction of the fatigue life using fracture-mechanics concepts, and Eq. 1 expresses the statistical mean line of the relevant fatigue test data shown by the solid circles in Figure 2. The following assumptions were made to assist with the evaluation of the crack-growth constants, C and n.

1. The crack was assumed to be described by a disc-like penny-shaped crack with a constant correction factor, f(a), over the interval of integration. The correction factor, f(a), for a penny-shaped crack is $2/\pi$.
2. The estimates of the initial and final crack radii, a_i and a_j, were available from visual observations. The average initial crack radius, a_i, was assumed to equal the estimate of the equivalent crack radius, $a_e = 0.04$ in., which represents the sample of measured pores. The final crack radius, a_j, was assumed to be reached when the crack had penetrated the extreme fiber of the flange. The life remaining after this occurred was at most 10 percent of the total fatigue life of the beam as was shown by the measurements given in Figure 3. The final crack radius was assumed to be equal to the nominal flange thickness. Experimental observations indicated this to be reasonable.
3. It was assumed that all three grades of steel could be represented by the same crack-growth equation. This assumption was based on results of tests on the welded beams. It was shown elsewhere (4) that grade of steel did not significantly influence the fatigue life of the beams.

If we equate the values of the coefficients for the mean regression curve (Eq. 1) to the coefficients n and C' (Eq. 7) and substitute the crack radii, a_i and a_j, and the correction factor, f(a), into Eq. 6, the growth constants, $n \cong 3$ and $C = 2.05 \times 10^{-10}$, are derived. Substitution of these constants into Eq. 3 numerically describes the crack growth rate in terms of ΔK:

$$da/dN = 2.05 \times 10^{-10} \Delta K^3 \qquad (8)$$

The measurement used for crack-growth rates, da/dN, was inch/cycle; and for the stress-intensity factor range, ΔK, it was ksi$\sqrt{\text{in.}}$

COMPARISON OF DERIVED CRACK-GROWTH EQUATION WITH MEASURED CRACK-GROWTH RATES

Equation 8 as derived from the mean regression curve of fatigue test data (Fig. 2) is shown in Figure 7 and compared with the various stages of crack growth in the test beam shown in Figure 3. The straight-line estimate for crack growth as a penny-shaped crack from crack initiation until penetration of the extreme fiber is indicated. Also shown are the data points for the measured crack-growth rates on the inside and outside surface of the flange for growth as a three-ended crack.

It is apparent from Figures 7 and 3 that most of the life is spent growing the crack from its initial equivalent flaw radius, $a_e = 0.04$ in., to its penetration of the extreme fiber of the flange, $a_f = 0.375$ in. The corresponding range of ΔK for the test beam was between 8 ksi$\sqrt{\text{in.}}$ and 25 ksi$\sqrt{\text{in.}}$ under a constant amplitude stress range of 36 ksi while 435,000 cycles elapsed. The transition from a penny-shaped crack to a three-ended crack only required about 16,000 cycles. An additional 10,000 cycles were required to grow the crack large enough to cause net-section yielding. Final failure terminated testing at 467,000 cycles.

It is also apparent from Figure 7 that most of the life was spent while growth occurred in a region of small ΔK. This is particularly true for lower applied stress

Figure 4. Two small fatigue cracks that initiated from pores in the longitudinal fillet weld and grew perpendicular to the axis of the weld (~x5.5).

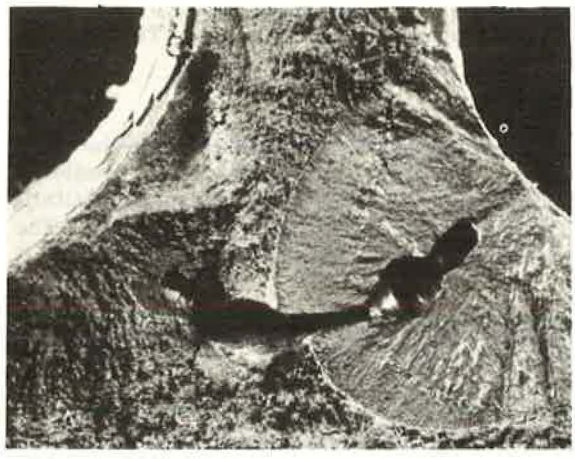

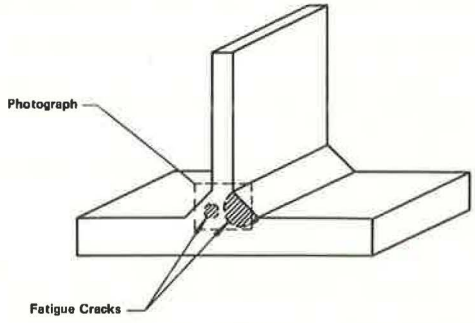

Figure 5. Small crack with penetration to the fillet weld surface (~x6.3).

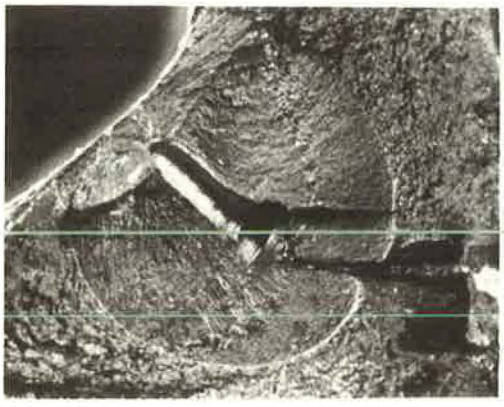

Figure 6. Crack in flange-to-web junction approaching the extreme fiber of the tension flange (~x2.1).

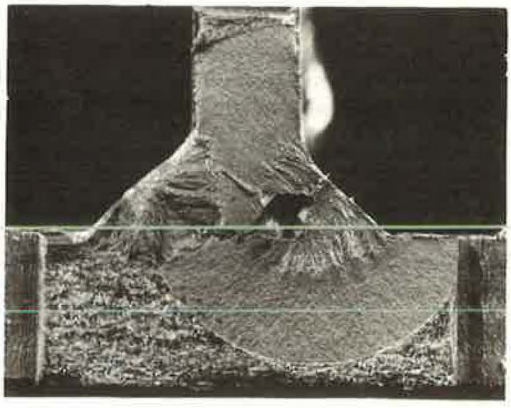

Figure 7. Stages of crack growth and corresponding growth rates for a crack in a plain-welded beam.

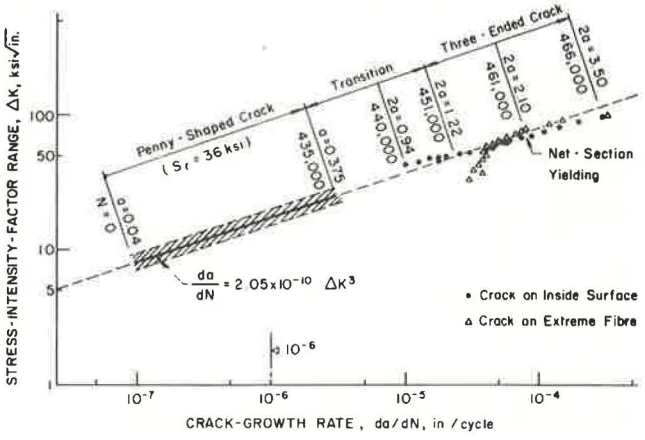

ranges as shown in Figure 8. The ΔK-regions applicable to growth as a penny-shaped crack are indicated for the test beams subjected to the stress ranges used in this study. Crack initiation took place at ΔK-values below 10 ksi $\sqrt{in.}$ in all test beams. Most of the life was spent at growth rates smaller than 10^{-6} in. per cycle.

The derived crack-growth relationship given by Eq. 8 is also compared with data from crack-growth specimens (Fig. 8). It was necessary to extrapolate the curve into the higher growth-rate region to compare it with available growth-rate data. The extrapolated curve falls within the scatterband reported by Crooker and Lange (3). This scatterband contains data from tests on carbon and low-alloy steels with yield strengths comparable to the yield strengths of the steel beams. A conservative upper bound for growth rates on ferrite-pearlite steels was proposed by Barsom (1) as

$$da/dN = 3.6 \times 10^{-10} \Delta K^3 \tag{9}$$

This relationship is parallel to Eq. 8.

Because much of the growth in the plain-welded beams took place in the weld metal and heat-affected zone, a comparison of the theoretical curve with Maddox's data (13) is relevant. An approximate envelope for Maddox's data on four different weld metals is shown. Three had about equal yield strength (67 ksi), and the fourth had a higher yield point equal to 90 ksi. Also included in the scatterband are test data for a simulated heat-affected zone in mild steel material with the same yield strength. The correlation with these crack-growth data is good.

It is apparent from Figure 8 that the Crooker-Lange scatterband does not cover the critical region of interest for plain-welded beams. Most studies of crack-growth rates have been limited to larger ΔK-values and higher crack-growth rates because of the difficulties encountered in the slow-growth region. However, the theoretical curve (Eq. 8) extrapolated into the higher ΔK-regions shows the same general trend reported by others on basic crack-growth specimens (Fig. 8). The theoretical curve is just above the crack-growth data and underestimates their growth rate. This is surprising because the penny-shaped crack assumes the best condition for the crack in the welded beams and neglects the influence of free surfaces. This underestimate in growth rate may be due to crack initiation or an overestimate of the stress intensity.

The exponent, n, of the predicted crack-growth equation was about equal to 3.00 (Eq. 8). It represents the slope of the fatigue test data on plain-welded beams fabricated from three grades of steel. Crooker and Lange (3) observed from a review of the literature that the value of the slope, n, fell between 2 and 4 for a large range of steels. Gurney (6) reported the slope of the curve to be a linear function of yield stress of the material. A general trend observed in crack-growth studies is for the value of the exponent, n, to decrease with increasing yield strength of the material. This trend was not as pronounced in the welded-beam study. The value of the exponent, n, did not appear to vary greatly from 3.

Careful evaluation of the coefficients n and C is needed for a wider range of rates of growth. Most of the data generally used to fit the straight-line approximation only extend over a small range of ΔK. In other cases, data points at the extremes cause rotation of the line. Substantial overestimates or underestimates of the fatigue life of a structural component might result if crack-growth relationships are used to extrapolate beyond the range of the test data.

Very Slow Growth

Johnson and Paris (12) have suggested that a threshold exists for crack growth. A recent investigation by Paris (16) on ASTM 9310 steel has provided more information on this phenomenon of very slow growth. An approximate mean line fit to Paris' data is compared in Figure 9 and Eq. 8. A drastically reduced growth rate for $\Delta K \cong 5.2$ ksi $\sqrt{in.}$ is observed. Deviations from the straight-line approximation are also found for large ΔK-values, which indicates an increased growth rate and applies mainly to low-cylce fatigue problems.

Harrison (7) has reviewed the literature for runout data on a variety of specimens. He concluded that "for all materials with the exception of pure aluminum, cracks will

not propagate if $\Delta K/E < 1 \times 10^{-4} \sqrt{in.}$" Harrison's runout levels for four types of steel are also shown in Figure 9 and range between 3.3 ksi $\sqrt{in.}$ for mild steel and 5.3 ksi $\sqrt{in.}$ for austenitic steel.

Predictions of Fatigue Life Using Different Crack Models

Additional crack models were used to assess their influence on the prediction of the fatigue life. Figure 10 shows the results for the various models used. Six A441 steel beams were selected for the comparison. The actually observed fatigue lives of these six beams are shown by solid circles together with the mean and the 95 percent confidence interval for all test beams failing from porosity.

The defects that caused crack growth and failure of the six beams were examined. They were assumed to be characterized by a circumscribed ellipse with half-axes a and b. The following models were used to estimate the fatigue life of each individual beam by using the known dimensions of the circumscribed ellipse and the crack-growth Eq. 8.

The open circles shown in Figure 10 (model a) correspond to the life estimates for the penny-shaped crack with equivalent crack radius. The equivalent crack radius was computed from the equivalence of the K-value with the circumscribed elliptical crack.

Penny-shaped cracks were assumed to inscribe and circumscribe the ellipse. The shortest life estimates resulted from the circumscribed crack and the longest from the inscribed crack. These two estimates constitute "upper and lower bounds" and are indicated by the horizontal T-symbols shown in Figure 10 (model b).

Additional life estimates were made based on the elliptical crack model. Growth was assumed in the direction of the minor axis 2a with constant major axis 2b until the size of the circumscribed crack was reached. The computation of the increment of life from an elliptical to a circular crack was done by using an available computer program (5). Numerical integration was employed because of the variable correction factor, f(a). This increment of life was added to the estimate for the circumscribed penny-shaped crack. The total life estimate is indicated by the triangles shown in Figure 10.

The comparison between the estimates for each individual beam provided by the different models and the observed fatigue life permit the following observations.

1. The observed fatigue data were contained within the bounds from the estimates of the circumscribed and inscribed circles in all but one case.
2. Most of the estimates from models a and c fell within the two limits of dispersion representing the 95 percent confidence interval of all the beam test data. Hence, the selection of a penny-shaped crack model did not introduce more scatter than was experimentally observed from fatigue test data.

Prediction of Fatigue Life Using Measured Crack-Growth Rates

Maddox (14) and Harrison (8) have demonstrated that good predictions of the fatigue life can be obtained from crack-growth data. Barsom's (1) conservative estimate of crack-growth rate, Eq. 9, for ferrite-pearlite steels was used to predict the fatigue life of the beams failing from porosity. The result is shown in Figure 11 together with the applicable welded beam test data, the corresponding mean line, and 95 percent confidence interval.

Also shown in Figure 11 is the prediction based on Paris' data (16), which indicates a threshold level for runout at about 23 ksi. This prediction was obtained by using the straight-line segments shown in Figure 9, which approximate the data from the study on very slow growth. The threshold values by Harrison (7), also shown in Figure 9, were used to estimate runout. Runout tests are predicted to occur at levels as high as 20 ksi for low-alloy steel, as shown by the horizontal lines in Figure 11.

The predictions based on the crack-growth data underestimate the mean fatigue life of the test beams at the higher stress range levels. This was expected from the comparison of the crack-growth data. Because any assumption other than the penny-shaped crack model for the welded beams would further reduce the life prediction based on crack-growth data, a crack-initiation period may be responsible for the slight

Figure 8. Ranges for crack growth as a penny-shaped crack.

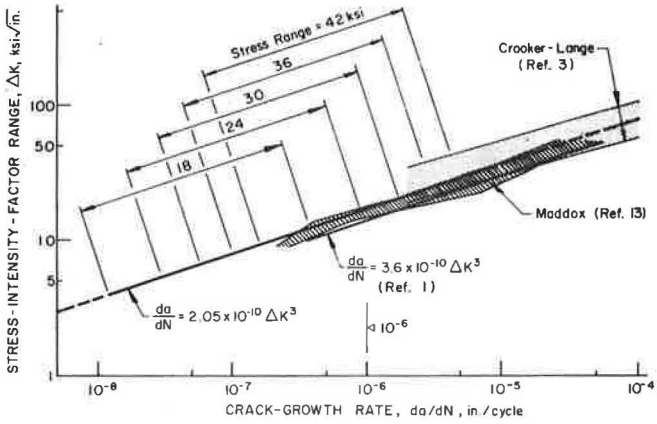

Figure 9. Approximate mean line of Paris' data for very slow growth and Harrision's limiting ΔK-values for nonpropagating cracks.

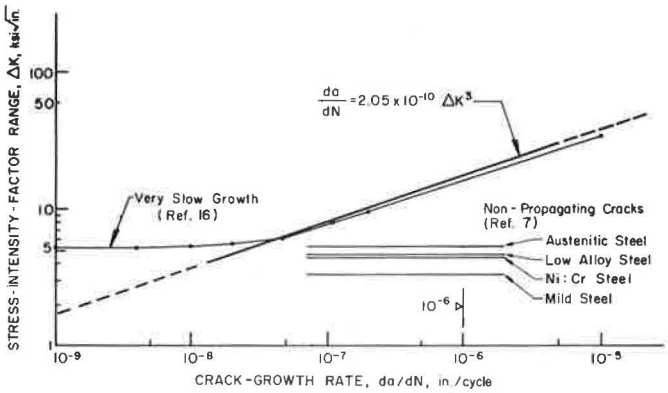

Figure 10. Prediction of fatigue life using crack models.

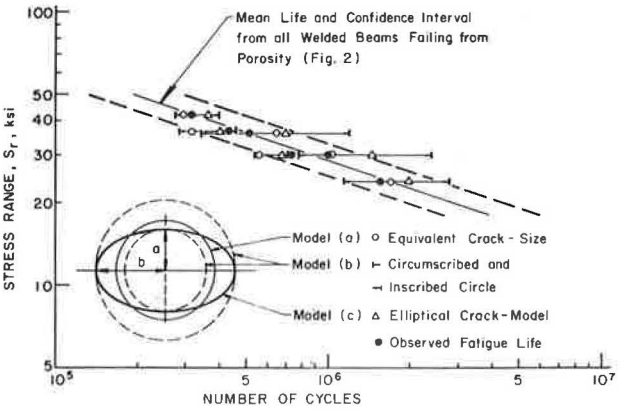

Figure 11. Comparison of a predicted low bound and a mean line with mean life and scatterband from test data.

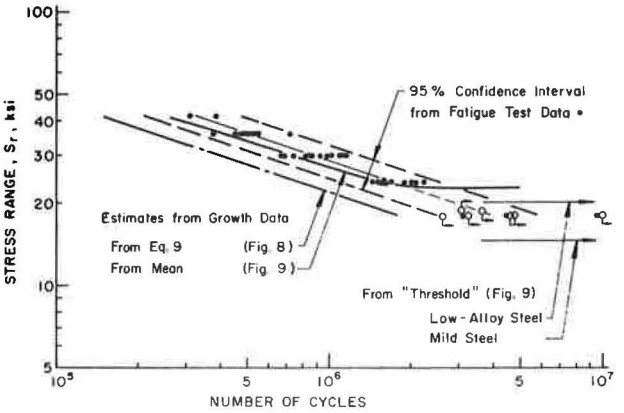

underestimate. Other factors that could be responsible for the underestimate in life are an overestimate of the initial crack size, an overestimate of the stress intensity, and a slower growth rate under plane-strain conditions (2).

The scatter in the test data shown in Figure 11 was previously related to the variation in shape, size, and severity of the porosity. Other factors contribute to the variation in test data. Beams with seemingly equal defects still experience variation in the fatigue strength because of variation in the crack-tip radius, crack-growth rates, and other uncontrolled variables.

SUMMARY AND CONCLUSIONS

The following findings of this study are based on a detailed examination of the test data, fracture surfaces, initial flaw conditions provided by the experimental work, and the theoretical studies of stable crack growth.

1. Fractographic examination of the initial flaw conditions revealed porosity to be the most common defect in plain-welded beams. The distribution of the size and location of the pores in the longitudinal fillet weld was random. The welded-beam fatigue data fell within a narrow scatterband when plotted as the logarithmic transformation of stress range and cycles to failure.
2. Fracture-mechanics concepts provided a rational way to analyze and characterize the behavior of welded beams. These concepts were applied to describe numerically the effective initial flaw conditions in welded beams and to derive a crack-growth rate versus range of stress-intensity relationship from welded-beam fatigue data.
3. A penny-shaped crack was found to model crack growth from porosity in welded beams. An equivalent crack with a 0.04-in. radius described the average pores observed in the welded beams.
4. The derived crack-growth equation exhibited the same trend as measured data from crack-growth specimens. It provided a lower estimate of the growth rate. Among other factors, this difference was attributed to crack initiation, a possible overestimate of the stress intensity, and slower growth in the plane-strain condition for the welded beams.
5. Available crack growth data were shown to only cover a small region of growth rates. Extrapolation into regions outside the data could be misleading, particularly when used for fatigue-life estimates.
6. Very little information is available for growth rates below 10^{-6} in. per cycle. This was found to be the region most critical for the fatigue behavior of welded and rolled beams. More than 75 percent of the life was spent in this region growing a crack from its initial size to a visible crack.
7. It was shown that the initial flaw size was the controlling factor for the fatigue life of welded beams. An increase in flange thickness and larger weld sizes should not result in an increase in allowable defect size.
8. The variation of the fatigue data within the scatterband was found to be related in part to the variation in the initial flaw condition and in part to the variation in fatigue crack-growth rates or other uncontrolled variables.

ACKNOWLEDGMENTS

This paper is based in part on the experimental and theoretical investigations made during the course of a research program on the effect of weldments on the fatigue strength of steel beams. Partial support was also provided by the Office of Naval Research, Department of Defense, under Contract N00014-68-A-514; NR064-509. The experimental research was performed under National Highway Research Program Project 12-7 at Fritz Engineering Laboratory, Department of Civil Engineering, Lehigh University, Bethlehem, Pennsylvania. The authors wish to express their appreciation for the helpful suggestions made by G. R. Irwin, A. W. Pense, and R. W. Hertzberg on the fracture mechanics and metallurgical aspects of this work. Special thanks are due Karl H. Frank and Ben T. Yen for their cooperation during the progress of this study.

REFERENCES

1. Barsom, J. M. Fatigue-Crack Propagation in Steels of Various Yield Strengths. U.S. Steel Corp., Applied Research Laboratory, Monroeville, Pennsylvania, 1971.
2. Clark, W. G., Jr., and Trout, H. E., Jr. Influence of Temperature and Section Size on Fatigue Crack Growth Behavior in Ni-Mo-V Alloy Steel. Engineering Fracture Mechanics, Vol. 2, No. 2, Nov. 1970, pp. 107-123.
3. Crooker, T. W., and Lange, E. A. How Yield Strength and Fracture Toughness Considerations Can Influence Fatigue Design Procedures for Structural Steels. Welding Research Supplement, Vol. 49, No. 10, Oct. 1970, pp. 488-496.
4. Fisher, J. W., Frank, K. H., Hirt, M. A., and McNamee, B. M. Effect of Weldments on the Fatigue Strength of Steel Beams. NCHRP Rept. 102, 1970, 112 pp.
5. Frank, K. H., and Fisher, J. W. Analysis of Error in Determining Fatigue Crack Growth Rates. Lehigh University, Fritz Engineering Laboratory, Rept. 358.10, March 1971.
6. Gurney, T. R. An Investigation of the Rate of Propagation of Fatigue Cracks in a Range of Steels. The Welding Institute, Members' Rept. E18/12/68, Dec. 1968.
7. Harrison, J. D. An Analysis of Data on Non-Propagating Fatigue Cracks on a Fracture Mechanics Basis. Metal Construction and British Welding Jour., Vol. 2, No. 3, March 1970, pp. 93-98.
8. Harrison, J. D. The Analysis of Fatigue Test Results for Butt Welds With Lack of Penetration Defects Using a Fracture Mechanics Approach. Welding in the World, Vol. 8, No. 3, 1970, pp. 168-181.
9. Hirt, M. A., Yen, B. T., and Fisher, J. W. Fatigue Strength of Rolled and Welded Steel Beams. ASCE, Jour. Struct. Div., Vol. 97, No. ST7, July 1971, pp. 1897-1911.
10. Hirt, M. A. Fatigue Behavior of Rolled and Welded Beams. Lehigh University, Department of Civil Engineering, PhD dissertation, Oct. 1971.
11. Irwin, G. R. Analysis of Stresses and Strains Near the End of a Crack Traversing a Plate. Transactions, ASME, Series E, Vol. 24, No. 3, Sept. 1957, pp. 361-364.
12. Johnson, H. H., and Paris, P. C. Sub-Critical Flaw Growth. Engineering Fracture Mechanics, Vol. 1, No. 1, June 1968, pp. 3-45.
13. Maddox, S. J. Fatigue Crack Propagation in Weld Metal and Heat Affected Zone Material. The Welding Institute, Members' Rept. E/29/69, Dec. 1969.
14. Maddox, S. J. The Propagation of Part-Through-Thickness Fatigue Cracks Analysed by Means of Fracture Mechanics. The Welding Institute, Members' Rept. E/30/69, Dec. 1969.
15. Paris, P. C. The Fracture Mechanics Approach to Fatigue. Proc., Tenth Sagamore Army Materials Research Conference, Syracuse University Press, Syracuse, 1964, p. 107.
16. Paris, P. C. Testing for Very Slow Growth of Fatigue Cracks. Closed Loop, MTS Systems Corp., Vol. 2, No. 5, 1970, pp. 11-14.